Epilepsia, 49(5):772–785, 2008
doi: 10.1111/j.1528-1167.2007.01436.x

FULL-LENGTH ORIGINAL RESEARCH

Voxel-based 3D MRI analysis helps to detect subtle forms of subcortical band heterotopia

*Hans-Jürgen Huppertz, †Jörg Wellmer, ‡Anke Maren Staack, §Dirk-Matthias Altenmüller, ¶Horst Urbach, and *Judith Kröll

*Swiss Epilepsy Centre, Zürich, Switzerland; †Department of Epileptology, University of Bonn, Bonn, Germany; ‡Epilepsiezentrum Kork, Kehl-Kork, Germany; §Epilepsy Center, University Hospital Freiburg, Freiburg, Germany; and ¶Department of Radiology/Neuroradiology, University of Bonn, Bonn, Germany

SUMMARY

Purpose: To evaluate the potential diagnostic value of a novel magnetic resonance image (MRI) postprocessing technique in subtle forms of subcortical band heterotopia (SBH). The method was introduced to improve the visualization of blurred gray–white matter junctions associated with focal cortical dysplasia but was found to be applicable also to SBH.

Methods: In the voxel-based MRI analysis presented here, T_1-weighted MRI volume data sets are normalized and segmented using standard algorithms of SPM5. The distribution of gray and white matter is analyzed on a voxelwise basis and compared with a normal database of 150 controls. Based on this analysis, a three-dimensional feature map is created that highlights brain areas if their signal intensities fall within the range between normal gray and white matter and differ from the normal database in this respect. The method was applied to the MRI data of 378 patients with focal epilepsy in three different epilepsy centers.

Results: SBH was diagnosed in seven patients with five of them showing subtle forms of SBH that had gone unrecognized in conventional visual analysis of MRI and were only detected by MRI postprocessing. In contrast to distinct double cortex syndrome, these patients had partial double cortex with SBH mostly confined to posterior brain regions.

Conclusions: The results of this study suggest that a considerable part of cases with SBH might remain unrecognized by conventional MRI. Voxel-based MRI analysis may help to identify subtle forms and appears to be a valuable additional diagnostic tool in the evaluation of patients with cryptogenic epilepsy.

KEY WORDS: Subcortical band heterotopia, Double cortex, Cryptogenic focal epilepsy, MRI, Postprocessing, Cortical malformation, Neuronal migration disorder.

We have recently proposed a new voxel-based method for postprocessing of magnetic resonance images (MRIs) in order to improve the recognition and delineation of focal cortical dysplasia (FCD) (Huppertz et al., 2005). The method is based on algorithms of SPM (statistical parametric mapping software, Wellcome Department of Imaging Neuroscience Group, London, U.K., http://www.fil.ion.ucl.ac.uk/spm) and was developed to highlight brain regions with blurring, that is, disturbed differentiation of the gray–white matter junction that is frequently associated with FCD. The utility of this technique, however, is not limited to FCD. In cases of double cortex syndrome, a neuronal migration disorder associated with medically intractable epilepsy and mental retardation (Barkovich et al., 1989; Palmini et al., 1991; Barkovich & Kuzniecky, 2000; D'Agostino et al., 2002; Barkovich et al., 2005), the subcortical band heterotopia (SBH) underlying the cortex are also accentuated by this method, possibly because of slightly higher voxel intensities compared to normal cortex and/or partial volume effects at the border of the abnormally localized gray matter (GM) that are enhanced by the algorithm of this method. However, the recognition of a distinct double cortex syndrome with diffuse SBH throughout the whole brain usually does not pose a diagnostic problem or require a special postprocessing of

Accepted October 17, 2007; Online Early publication November 30, 2007.

Address correspondence to Hans-Jürgen Huppertz, M.D., Swiss Epilepsy Centre, Bleulerstrasse 60, CH-8008 Zürich, Switzerland. E-mail: hans-juergen.huppertz@swissepi.ch

Blackwell Publishing, Inc.

the MRI data. But there seem to be other cases with a syndrome of partial double cortex and only subtle forms of thin and sometimes discontinuous SBH (Sicca et al., 2003) that can be difficult to detect in conventional MRIs. A patient with cryptogenic focal epilepsy who had already received a presurgical evaluation at the Department of Epileptology of the University of Bonn (Germany) became our index patient when a postprocesssing of his MRI revealed double cortex syndrome that had not been detected in previous MRI examinations. Subsequently, we tried to determine other cases of subtle SBH that had gone unrecognized in conventional visual analysis of MRI and had only been detected by voxel-based MRI analysis. This was done in order to assess the prevalence of this syndrome, to determine clinical and imaging properties, and to evaluate the potential diagnostic value of our MRI postprocessing technique for this kind of cortical malformation.

Methods

Patients and normal database

The patients reported here have been collected in three different epilepsy centers, that is, the Swiss Epilepsy Centre in Zurich (Switzerland), the Epilepsiezentrum Kork in Kehl (Germany), and the Department of Epileptology of the University of Bonn (Germany). In the Swiss Epilepsy Centre, a register has been maintained for all patients receiving an MRI since January 2006. Voxel-based MRI analysis as described later has been applied to all patients with focal cryptogenic epilepsy for whom a T_1-weighted volume data set was available in digital form in sufficient quality. In addition, a subgroup of patients with focal symptomatic epilepsy (i.e., with already known epileptogenic lesion) was analyzed, for example, to determine the extent of cortical malformations or to exclude dual pathology in cases of hippocampal sclerosis. Exclusion criteria for MRI postprocessing were gross movement artifacts or extensive lesions (e.g., brain infarct areas, large postoperative defects, posttraumatic lesions) that would have disturbed the normalization and segmentation of the image. The register was searched for all cases of SBH detected either by conventional MRI or voxel-based MRI analysis, respectively. In the Department of Epileptology of the University of Bonn and in the Epilepsiezentrum Kork, MRI postprocessing has been used only for selected cases of focal cryptogenic epilepsy. These patient groups were also searched for cases of SBH, but because of the inconstant use of the method, assessing the prevalence in these populations was not appropriate.

The MRI data were acquired on different MRI scanners of 1.5 and 3 Tesla (T), that is, Philips Achieva 3T (Zurich), Siemens Symphony 1.5T (Kehl-Kork), and Siemens Trio 3T (Bonn). Apart from the T_1-weighted MRI volume data sets used for the postprocessing described later, the protocols for the high-resolution MRI acquisitions of these patients comprised at least the following sequences: fluid-attenuated inversion recovery (FLAIR) images (slice thickness, 5–6 mm axial and 2–3 mm coronar), T_1-weighted images (2–3 mm coronar, and for Kehl-Kork also 2 mm sagittal and axial), T_2* images (slice thickness, 5–6 mm axial), and T_2-weighted images with gadolinium-DTPA (slice thickness, 5–6 mm axial).

The MRI postprocessing requires the comparison of individual patient images with the MRI data of a normal database. The latter consisted of 150 controls (70 female, 80 male, with ages ranging from 15 to 77 years and a mean age of 30.9 $\pm$ 9.6years). A subgroup of 30 controls comprised patients who were referred to the Swiss Epilepsy Centre to investigate paroxysmal events of unknown etiology and turned out to suffer from nonepileptic psychogenic seizures or syncopes. The other 120 controls were healthy subjects without current or past neurological or psychiatric disease. The T_1-weighted MRI volume data sets for postprocessing were acquired on five different MRI scanners, that is, Siemen Sonata 1.5T, (Siemens, Munich, Germany) Siemens Magnetom Vision 1.5T, Siemens Avanto 1.5T, Siemens Trio 3T, and Philips Intera (Philips, Amsterdam, The Netherlands) with 30 MRI data sets from each scanner. All images were thoroughly inspected and were found to be free of structural abnormalities. Procedures were in accordance with local institutional review board requirements.

MRI postprocessing

The MRI postprocessing presented here is based on standard procedures available within SPM5 (e.g., normalization, segmentation) and additional simple computations by the image calculation tool of SPM5 (e.g., calculation of a difference image, conversion to a binary image, masking). It is fully automated using a MATLAB (MathWorks, Natick, MA, U.S.A.) batch script. The starting point is a high-resolution T_1-weighted MRI volume data set containing the whole head. The data set is transferred in digital imaging and communication (DICOM) format from the MR scanner to an AMD Opteron 2.0 GHz PC and converted to ANALYZE format by means of the DICOM conversion tool of SPM5. For each patient, a so-called junction image that highlights brain regions with disturbed differentiation of the gray–white matter junction is derived from the original T_1 image. The calculation of the junction image includes the following steps (see also Fig. 1; the numbers within the figure correspond to the following processing steps):

Normalization and intensity correction, and simultaneous Segmentation

SPM5 includes a probabilistic framework (called "unified segmentation") whereby image registration, tissue classification, and bias correction are integrated within the same generative model (Ashburner & Friston, 2005). By

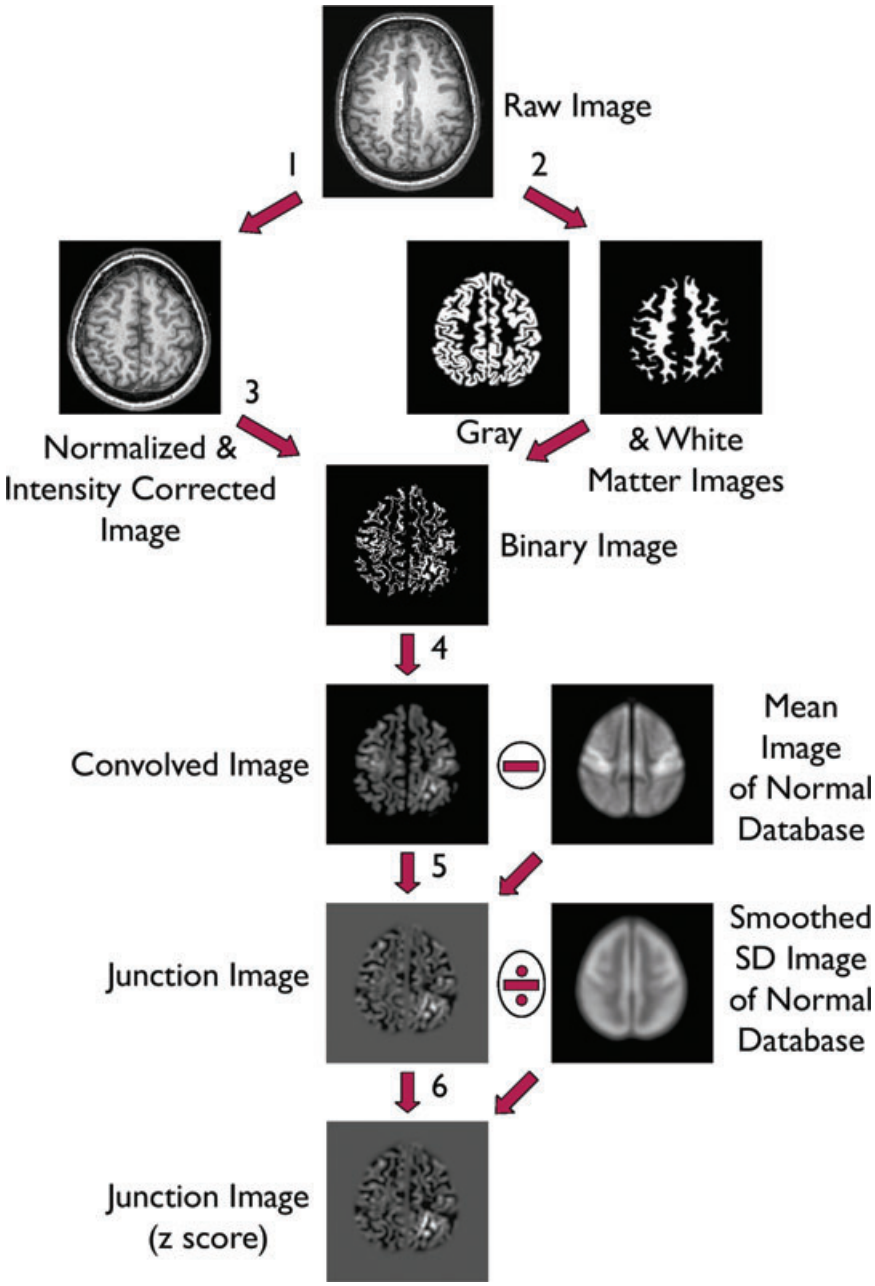

Figure 1.
Overview of the image processing steps required for calculating the junction image: (1) normalization, (2) segmentation and intensity correction, (3) conversion to a binary image, (4) convolution, (5) comparison with the normal database (NDB), and (6) calculation of the z-score image (see text for details).
Epilepsia © ILAE

using this framework, the 3D MRI data set of each patient is normalized to the standard brain of the Montreal Neurological Institute (MNI) included in the SPM5 distribution, segmented into different brain compartments, that is, GM, white matter (WM), and cerebrospinal fluid, and simultaneously corrected for small intensity inhomogeneities. This "unified segmentation" step uses the following default parameters: warping regularization = 1; warp frequency cutoff = 25; bias regularization = 0.0001; bias FWHM = 60; voxel size = 1 × 1 × 1 mm (please cf. the SPM5 manual for a more detailed explanation). However, the number of Gaussians used to represent the intensity distribution for each tissue class has been changed for the calculation of the junction image. Instead of using two Gaussians for GM, two for WM, two for CSF, and four for everything else, as recommended in the SPM manual, we have chosen only one Gaussian for gray and white matter, respectively, to get unambiguous results for the means and standard deviations of the voxel intensities in these tissue classes.

Conversion to binary image

The means and standard deviations of the voxel intensities in the gray and white matter compartments are used to determine individual upper and lower intensity thresholds

for the conversion of the normalized and intensity corrected image to a binary image. The thresholds are given by the functions

$$T_{LowerThreshold} = Mean_{GM} + 1/2 SD_{GM}$$

and

$$T_{UpperThreshold} = Mean_{WM} - 1/2 SD_{WM}$$

with "Mean" and "SD" as mean and standard deviation of the voxel intensities in the respective tissue class. Each voxel with a gray value between these thresholds is set to 1 in the resulting binary image, while the other voxels are set to zero. In addition, noncortical brain regions like basal ganglia, brainstem, and cerebellum are masked out by a predefined mask. The latter is derived from the "aal" image included in the MRIcro distribution and provided by Tzourio-Mazoyer et al. (Rorden & Brett, 2000; Tzourio-Mazoyer et al., 2002).

Convolution

The binary image is filtered by performing a three-dimensional (3D) convolution with a cubic matrix (convolution kernel) of 5^3 ones. As a result, brain regions where voxels of value 1 are clustered appear bright in the convolved image.

Comparison with normal database

To compensate for the variability of the gray–white matter transition zone in different brain regions, the convolved patient image is compared with the normal database. The MR data sets of the controls forming our normal database were processed in the same way as described in steps 1–4 and then averaged. The resulting mean image is subtracted voxel by voxel from the convolved patient image to obtain the junction image. Bright regions in this junction image primarily correspond to cortical areas of less defined border between gray and white matter and broader transition zone as compared to the normal database. However, other brain areas (e.g., subcortical structures) may be highlighted as well if their signal intensities fall within the range between normal gray and normal WM as defined in step 3 and differ from the normal database in this respect.

Calculation of z- score image

Apart from the mean image of the normal database, the convolved images of the controls were also used to calculate a "standard deviation (SD) image" providing standard deviations of the normal database for all voxels. In the last step, the junction image is divided by this SD image of the normal database to get a junction image with *z*-score normalized data. To avoid outlier values at the border of the standard brain where only few subjects contribute to the normal database and its standard deviation, the SD image was previously smoothed by using a fixed Gaussian kernel of 6-mm full width at half maximum (FWHM). The calculation of the *z*-score normalized junction image is aimed at further improving the visualization of brain regions that differ from the normal database concerning their voxel intensities (cf. Fig. 1).

RESULTS

Between January 2006 and August 2007, 756 patients of the Swiss Epilepsy Centre received an MRI according to the protocol described earlier. Based on clinical history, seizure semiology, and EEG findings, 499 of these patients were classified as suffering from focal epilepsy. MRI postprocessing was applied to 325 patients out of this group.

SBH were diagnosed in five patients, which amounts to a prevalence of about 1% in this population of patients with focal epilepsy referred to a tertiary epilepsy center. In two out of them (patients 1 and 2), the cortical malformations were recognized both in the conventional MR images and in MRI postprocessing. In three other patients (No. 4, 5, and 6), SBH were not detected until the junction images derived from voxel-based MRI analysis highlighted subcortical band-like structures parallel to the normal cortical ribbon. SBH were subsequently confirmed by reevaluation of the conventional MRI previously judged as normal. There was no patient with SBH who had gone unrecognized in the MRI postprocessing while being detected in the conventional MRI.

In the Department of Epileptology of the University of Bonn, only one patient with SBH was identified within a group of 30 patients analyzed since application of the postprocessing to cases of cryptogenic focal epilepsy. This was the index patient mentioned in the introduction (patient 3). In the Epilepsiezentrum Kork where voxel-based MRI analysis has been applied to 23 patients with cryptogenic focal epilepsy since January 2006, one patient was discovered by MRI postprocessing who is suspected of suffering from double cortex syndrome (patient 7).

An overview of clinical, electrophysiologic, and neuroradiologic data of the seven patients is presented in Table 1. There was no patient with a family history of mental retardation or epilepsy. In addition, there was no personal history of antenatal or perinatal complications. Apart from shallow sulci in patients 1 and 2, visual inspection and curvilinear reconstruction of the MRI data (Huppertz et al., 2007) did not reveal any accompanying malformation of the overlying cortex (e.g., no pachygyria or lissencephaly). More details are given later, with main emphasis on those patients with more subtle, incomplete, or only suspected SBH (patients 3–7). The findings in the T_1-weighted images and the MRI postprocessing of these patients, respectively, are presented in separate figures to allow the reader an unbiased evaluation of conventional MR images (Fig. 3) before referring to the corresponding junction images resulting from voxel-based analysis (Fig. 4) or the details in the enlarged images of Fig. 5, which pointed to the diagnosis of SBH. Furthermore, the patients in these

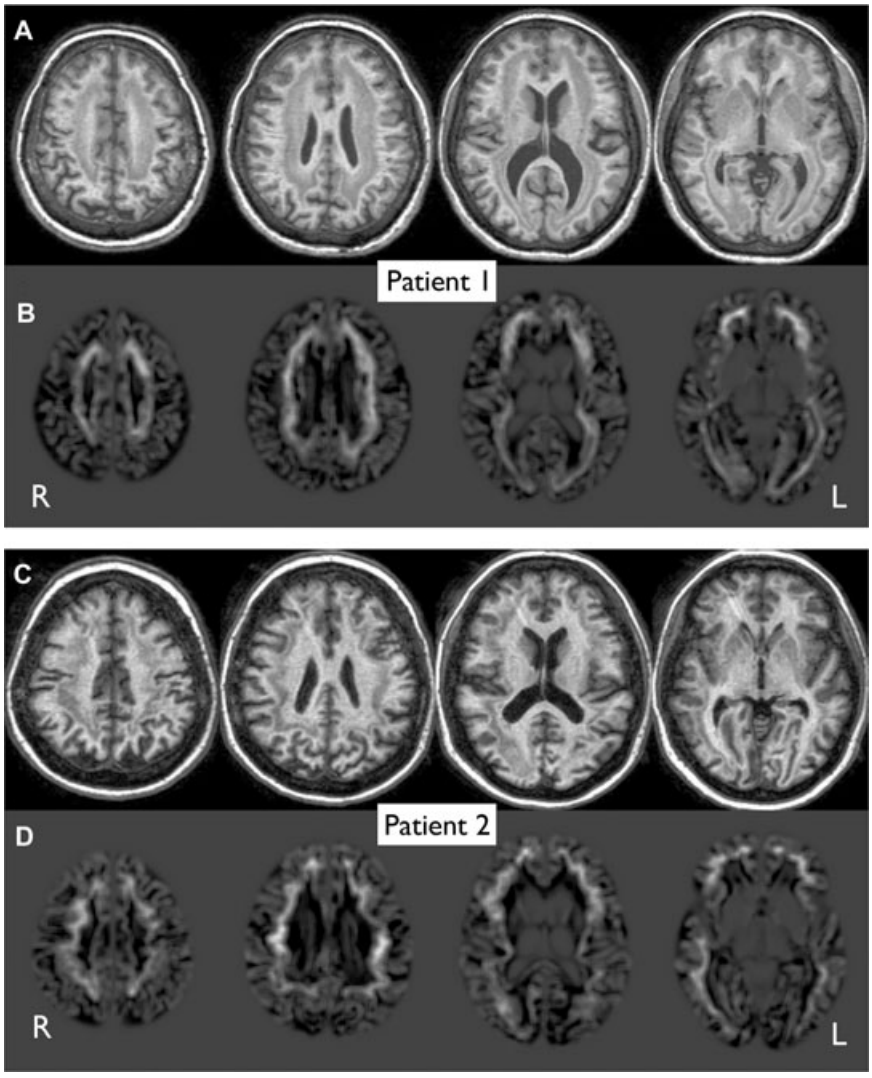

Figure 2.
Axial T_1-weighted MR images and corresponding results of voxel-based MRI analysis in two female patients with clearcut subcortical band heterotopia (SBH). In both patients, T_1-weighted images (row A and C) show continuous bilateral bands of heterotopic gray matter in between the cerebral cortex and the lateral ventricles, separated from both by white matter. In the junction images (row B and D), these areas of SBH are highlighted because their signal intensities fall in the range between normal gray and white matter and differ from the normal database in this respect. The overlying cerebral cortex appears normal both in the T_1-weighted and in the junction images except for shallow sulci in the frontal regions.

figures are ordered from (retrospectively) obvious to more subtle cases of SBH, finishing with patient 7 in whom this diagnosis is only suspected so far.

Patients 1 and 2

These two 36- and 40-year-old female patients had clearcut double cortex syndrome with a broad band of subcortical heterotopic GM throughout the brain and shallow sulci in the overlying cortex. Fig. 2 shows slices of the T_1-weighted MRI sequence and the corresponding results of voxel-based MRI analysis.

Patient 3

The 36-year-old female patient suffers from pharmacoresistant epilepsy since age 15. Seizure semiology includes elements suspicious for a temporal epileptogenic zone. Simple partial seizures go along with epigastric sensations and nausea, occasionally with weeping; complex-partial seizures comprise early oral automatisms, finger rubbing, reactionless starring, and loss of consciousness. Repeated MRI scans (many of them overlaid by motion artifacts) showed unspecific frontal WM lesions and a transient T_2 and FLAIR hyperintensity of the corpus callosum. Potentially epileptogenic lesions were not detected. Video-EEG monitoring during presurgical evaluation revealed ictal rhythmic activity mainly located in left temporo-posterior regions (electrode T5 > T3, T1, O1), while interictal epileptic activity was also found in the left anterior temporal and both frontal lobes. A SPECT examination did not deliver conclusive results. During a Wada test for identification of the underlying language dominance (result: strongly bilateral language organization), the patient developed a partial infarction of the left middle cerebral artery with a mild transient paresis of her right arm and mild aphasia. Symptoms completely ceased within 48 h. After this incident, the patient wished to interrupt the presurgical evaluation.

Table 1. Clinical, electrophysiologic, and neuroradiologic data in seven patients with SBH

Patient/ sex/age (years)/ clinic	Age at seizure onset (years)	Neurological examination/ psychology	Clinical seizure pattern	EEG	MRI
1/F/36 Zurich	8	Normal; MR	Hemianopsia R; CPS with oral and motor automatism; cloni + paraesthesia R; SG	I: temporal posterior L > temporal R, bifrontal; II: temporal posterior	Symmetric diffuse SBH throughout the brain; shallow sulci
2/F/40 Zurich	1	Normal; MR	CPS with clonic arm movements L; SG; psychogenic seizures	I: centro-temporal R II: temporal R	Symmetric diffuse SBH throughout the brain; shallow sulci
3/F/36 Bonn	15	Normal; MR	Epigastric aura; weeping; CPS with staring, oral and motor automatism	I: temporal anterior L > temporal L, bifrontal II: temporal posterior L	Asymmetric partial SBH with slight left posterior predominance
4/F/26 Zurich	10	Normal	Initial numbness of hand and arm R; CPS; SG	I: temporo-parietal L	Asymmetric partial SBH with posterior + left predominance; additional nodular heterotopia suspected
5/F/35 Zurich	12	Normal; MR	CPS with eye blinking, eye deviation to the left, oral + manual automatism; SG	I: temporo-occipital R >> temporal L and bifrontal II: temporo-parieto-occipital R	Symmetric partial SBH in posterior brain regions
6/M/42 Zurich	20	Normal	Metamorphopsia in the left visual field; CPS with oral and motor automatism	I: temporal posterior + parieto-occipital R+L II: parieto-occipital R+L	Symmetric partial subtle SBH in posterior brain regions
7/F/39 Kehl-Kork	18	Normal	Metamorphopsia and visual illusions; CPS with manual + oral automatism;SG	I: temporo-parieto-occipital R > L II: temporo-parieto-occipital R	Symmetric partial subtle SBH in posterior brain regions suspected

CPS, complex partial seizures; F, female; I, epileptiform potentials in interictal EEG; II, EEG seizure onset; L, left; M, male; MR, mild or moderate mental retardation; R, right; SBH, subcortical band heterotopia; SG, secondary generalization.

Six month later, the evaluation was continued. A new 3-Tesla MRI showed complete disappearance of the signs of the former infarction. When performing automated postprocessing of the new MRI subcortical signal alterations highly suspicious for a bihemispheric double cortex syndrome were found (Fig. 4, first row). Only after this hint, a reevaluation of the current and a previous MRI performed 6 months before confirmed the presence of a double cortex syndrome. Although the malformations showed a slight left posterior predominance (cf. Figs. 3–5, first row, column 4) correlating well with the EEG findings, the double cortex was clearly localized bilaterally. After this finding, the presurgical evaluation was terminated.

Patient 4

The 26-year-old female patient suffers from partial seizures with somatosensory symptoms with numbness of the right hand and secondary generalized tonic–clonic seizures since the age of 10 years. Partial seizures occur one to two times per month. There were no seizures recorded. Interictal EEG showed spike-waves in the left temporal and parietal regions. The patient's cognitive functions were normal (WAIS-R IQ 93).

A first MRI (1.5 T) at the age of 11 years was considered normal. With persisting seizures, a second MRI (3 T) was performed at the age of 25 years. A scattering of small cortex-isointense structures was found within the WM near the anterior horns of both lateral ventricles, suggesting nodular heterotopia (cf. Fig. 3, row 2, columns 2 and 3). SBH were only detected after additional voxel-based MRI analysis. This malformation appeared to be mainly localized in the left parietal lobe, hereby explaining seizure semiology and EEG results. However, MRI postprocessing revealed additional areas of thin and discontinuous SBH also in the contralateral right hemisphere (e.g., as shown in row 2, columns 2 and 3 of Figs. 4 and 5), thus confirming an asymmetric, but bilateral double cortex syndrome.

Patient 5

The 35-year-old female suffers from frequent partial seizures and tonic–clonic seizures since the age of 12 years. Partial seizures may start with an initial deviation of the eyes to the left, followed by oral and manual automatism, or only consist of eye blinking with short unresponsiveness. Ictal EEG demonstrated rhythmic beta activity over the right posterior region (electrodes P4, T6,

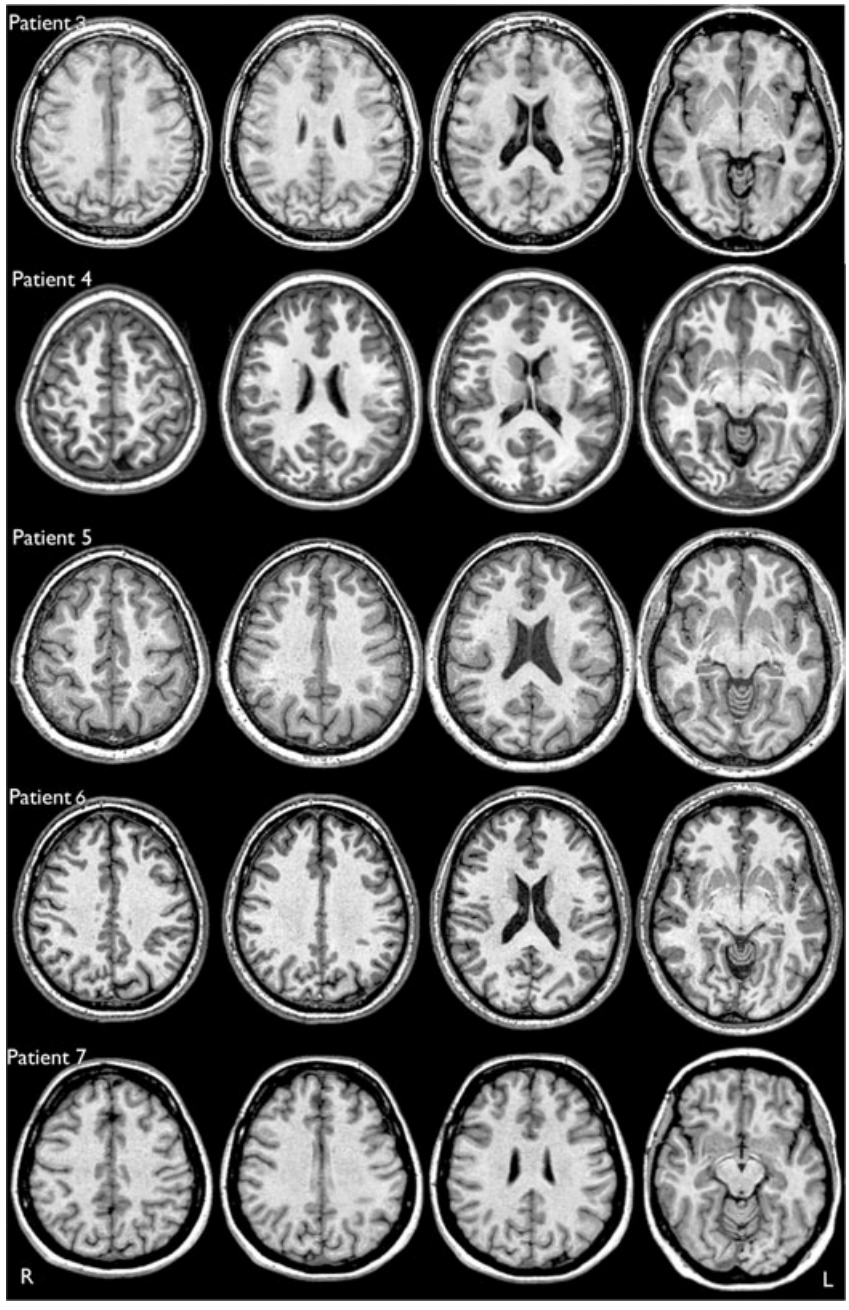

Figure 3.
Axial T_1-weighted MR images of 1-mm slice thickness shown in four different planes for each of the five patients with partial SBH who initially have not been recognized in the conventional MR images. The patients are arranged from (retrospectively) obvious to more subtle cases. In patient 7, SBH are only suspected because of very thin and hardly visible bandlike structures in both parietal and occipital lobes separated from the overlying cortex by a thin layer of white matter (please cf. also row 5 in Fig. 5).

and O2) followed by a diffuse electrodecremental phase. Interictal EEG showed frequent rhythmic sharp waves and a high-voltage rhythmic beta-activity during NREM-sleep over the right temporo-occipital region (T6, O2). There were less frequent independent spike waves over bifrontal and left temporal regions as well as a theta slowing in the same regions. IQ is below normal (WAIS-R IQ 60).

In two MRI investigations at the age of 18 and 26 years, no epileptogenic lesion was detected. With EEG being suggestive of a seizure onset in the right temporo-occipital region, two further MRI investigations (1.5 and 3T) were performed in 2005 and 2006 and demonstrated signal alterations in the posterior WM of both hemispheres in T_1- and T_2-weighted images that were interpreted as unspecific or possibly postinflammatory WM lesions (cf., Fig. 3, row 3). Only when voxel-based MRI analysis was applied to the latest MRI, it became obvious that these WM lesions were in fact a very broad band of heterotopic GM corresponding to a partial double cortex confined to the posterior parts of both hemispheres (Fig. 4, row 3). Retrospectively, the recognition of these malformations has been impeded for

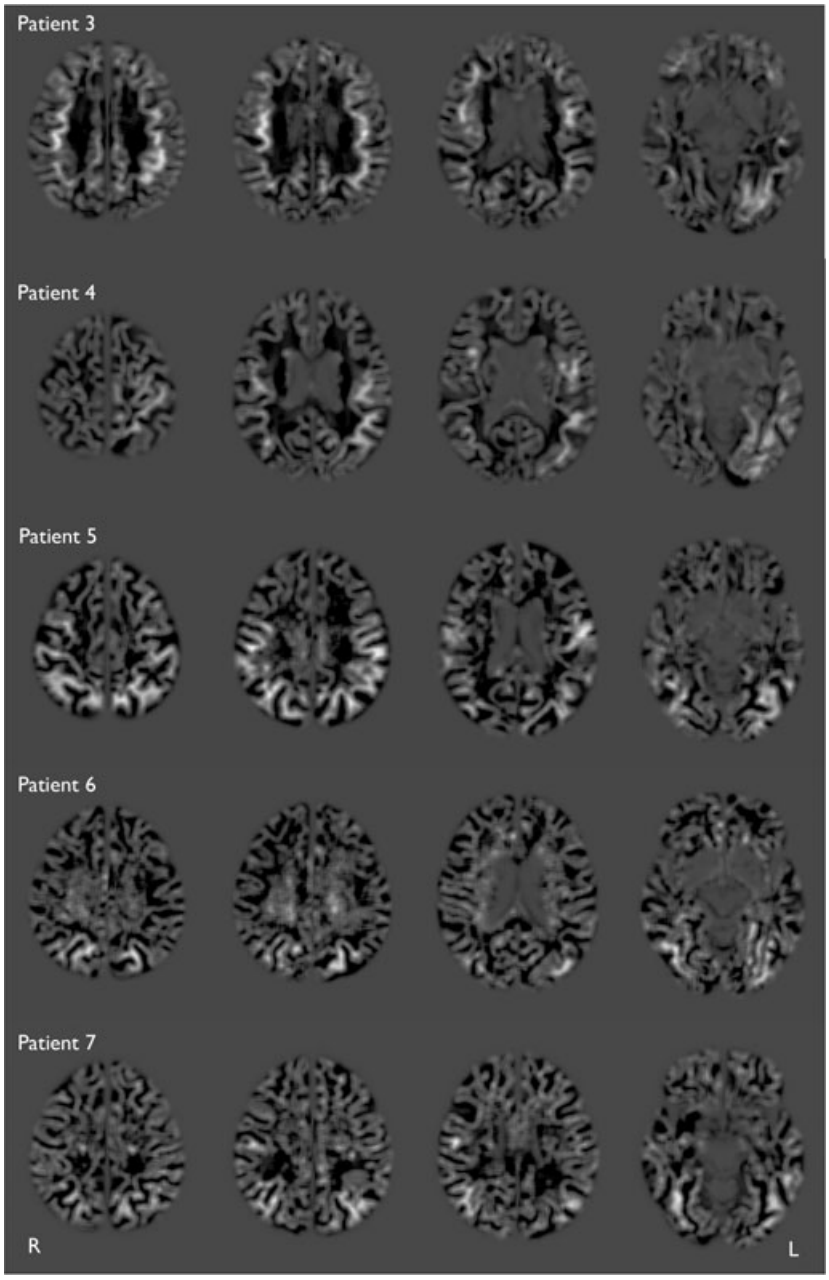

Figure 4.
MRI postprocessing results of the same five patients shown in Fig. 3. The junction images derived from the voxel-based MRI analysis highlight subcortical band-like structures suggestive of band heterotopia and were crucial for establishing the diagnoses in these patients. Please note that the method does not only aid to identify patients with subtle SBH but also help to assess the extent of these malformations and to verify the bilateral distribution, especially in cases with regional predominance (as in patient 4, e.g.).

a long time by their very symmetric distributions, which hampered a side comparison (cf., Fig. 5, row 3).

Patient 6

This 42-year-old businessman suffers from focal seizures since the age of 20 years. Seizures start with metamorphopsia in the patient's lower left visual field. These episodes last a few seconds and sometimes occur 4–10 times a week. Invariably, they are followed by a crossing of both arms over the chest, uttering of words, automatisms (oroalimentary, gestural, and/or continuation of preictal motor activity), a dystonic posture of one hand, and impaired consciousness. Ictal EEG demonstrated a nonlateralizing seizure pattern over the biposterior regions, and on interictal EEG, there were multiregional spike waves over the posterior temporal regions. Two MRI investigations, performed at the age of 22 years and 42 years, were considered normal. A voxel-based analysis applied to the second MRI (3 T) highlighted subcortical thin and discontinuous bandlike structures confined to the parietal and occipital lobes of both hemispheres (Fig. 4, row 4). After reevaluation of the MRI in these regions (Fig. 5, row 4), a partial double cortex syndrome with very subtle SBH in posterior brain regions was diagnosed,

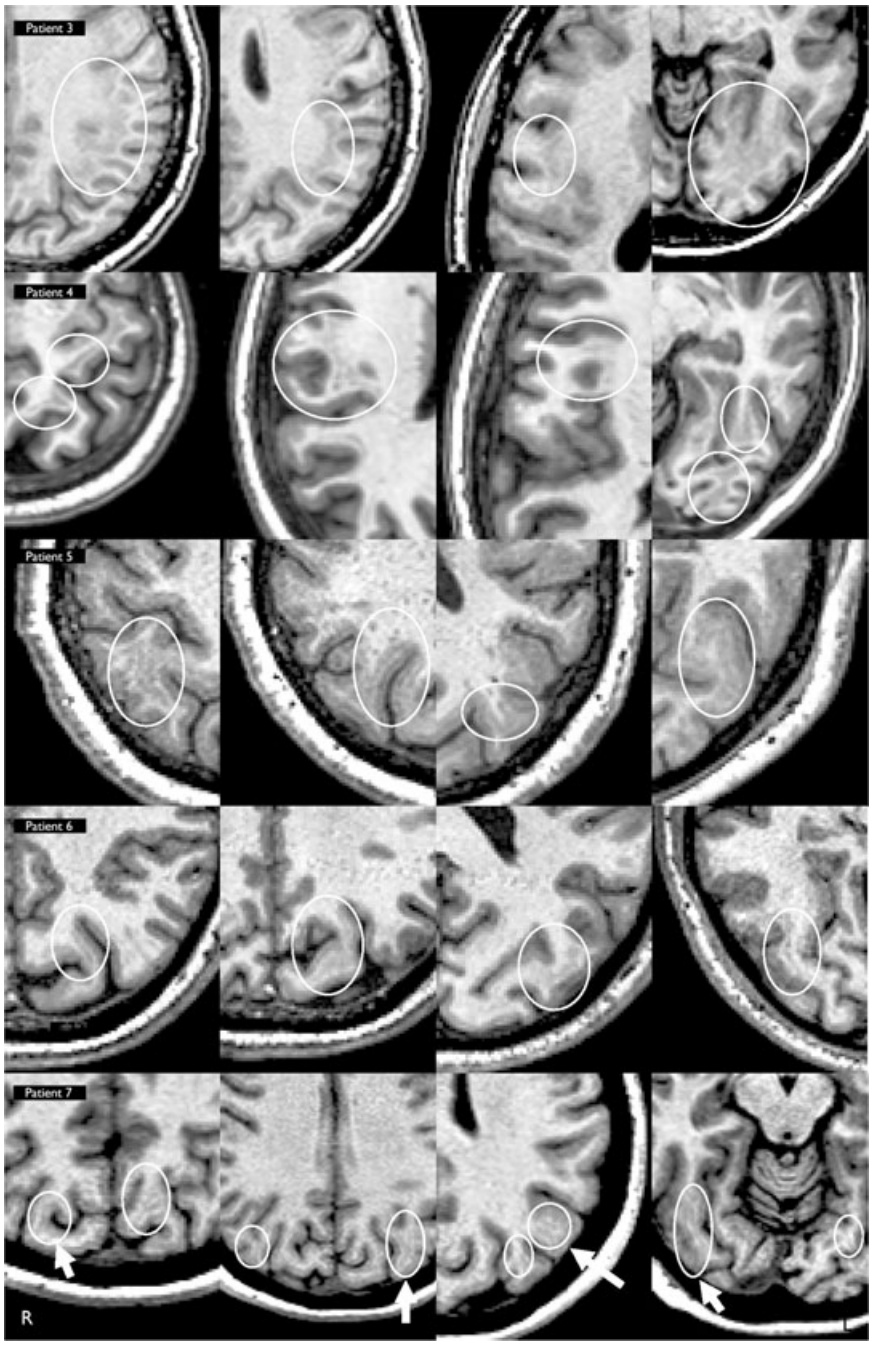

Figure 5.
Enlarged T_1-weighted MR images of Figs. 3 depicting characteristic imaging features of SBH in detail, and with the same order of patients as in Figs. 3 and 4 ranging from apparent to more subtle cases of SBH, finishing with patient 7 in whom the diagnosis is only suspected.
Epilepsia © ILAE

thus explaining very well ictal visual symptoms and EEG findings.

Patient 7

This 39-year-old female patient from the Epilepsiezentrum Kork has been suffering from focal pharmacoresistant epilepsy with simple partial visual, complex-partial, and infrequent secondary generalized tonic–clonic seizures for 21 years. Seizure semiology consisted of a visual aura with sudden light flashes without side preponderance and more complex symptoms, that is, a metamorphopsia of real objects or parts of the body with preserved visual acuity. In addition, the patient experienced visual illusions (e.g., an umbrella transforming into a dragon). The complex-partial seizures were characterized by initial smiling, loss of attention, ictal speech, oral and manual automatism, and short postictal reorientation.

In 1995, a resection of right mesiotemporal lobe structures was performed after video-EEG monitoring, which had shown right-sided ictal activity (semiinvasive

recording). Histological findings of the resected material did not show hippocampal sclerosis. Postoperatively, there was no change of seizure semiology or frequency. The patient reported on 30–40 seizures/month. Implantation of a vagal nerve stimulator did not affect the course of the disease.

Recent noninvasive EEG recordings showed mainly right-sided fast activity and temporoparietooccipital interictal epileptiform discharges. Infrequently, left-sided temporoparietooccipital slowing and spiking was visible as well. Ictal EEG demonstrated seizure onset at right temporoparietooccipital electrodes. The results of neuropsychological assessment (deficits in spatial orientation and perception of objects) indicated functional deficits in temporooccipital and temporoparietal regions of the nondominant hemisphere. MRI (1.5 T) revealed the lesion after resection of right amygdala and head of hippocampus. The hippocampal body and tail on the right side were preserved and showed no signs of sclerosis. No other lesions and especially no signs of cortical malformation were detected in conventional magnetic resonance imaging (Fig. 3, last row). MRI scans with higher field strength were not performed because of the vagal nerve stimulator. Positron-emission tomography showed a hypometabolism in the resected medial region of the right temporal lobe as the only abnormal finding.

Subsequent voxel-based MRI analysis highlighted bilateral subcortical thin and discontinuous bandlike structures in the parietal and occipital lobes (Figs. 4 and 5, last row), even more discrete than the findings in patient 4. While T_1- and FLAIR-weighted images showed no correlate, closer inspection of the high-resolution T_1 images revealed that these structures form tracks lying parallel to the gray–white matter junction but are divided from the normal cortex by a thin layer of WM (cf. Fig. 5, last row, circles with white arrows). These findings resembled very much the results in the other patients (e.g., when comparing the enlarged images of patients 5 and 7 in column 3 of Fig. 5) and pointed to the possibility of a very subtle form of double cortex.

Owing to the high frequency and pharmacoresistancy of the seizures and in view of the purely right-sided seizure origin indicated by noninvasive EEG, the patient was accepted for invasive EEG recordings at the Epilepsy Center of the University of Freiburg. Subdural strip electrodes were implanted over both parietal and occipital lobes as well as on the basal side of both hemispheres and in the posterior interhemispheric fissure. Invasive EEG demonstrated bilateral interictal epileptic activity with right-sided predominance. Clinically manifest seizures were found to start in both posterior brain regions below the implanted electrodes, and in contrast to the results of surface EEG with a slight left-sided predominance. Fig. 6 shows exemplarily a seizure with left-sided onset and early bilateral involvement of those regions where MRI postprocessing suggested the presence of SBH. The EEG curves are depicted in conjunction with 3-D visualization of electrode positions (Kovalev et al., 2005) and curvilinear reformatting of MRI (Huppertz et al., 2007).

With seizure onset zones documented in both hemispheres by invasive EEG recordings, the implanted electrodes were removed without resection. Besides, voxel-based analysis of an additional MRI acquired for the planning of implantation showed the same distribution of highlighted subcortical structures in the junction image as in the previous MRI postprocessing.

Discussion

In the present study, we report on the results of a new kind of voxel-based MRI analysis applied to epilepsy patients with SBH. The method has been primarily developed for improved visualization of blurred gray–white matter junctions associated with FCD. Because of the underlying algorithm, however, the method is not limited to FCD. Other structures may be highlighted as well if their signal intensities fall within the range between normal gray and white matter and differ from the normal database in this respect. In double cortex syndrome, the heterotopic band of GM is generally described as isointense with the cortical mantle in all imaging sequences (Barkovich et al., 1989). However, the intensities do not appear to be completely equivalent. In the T_1-weighted images of patients with clearcut double cortex syndrome shown in Fig. 2 (patients 1 and 2), the heterotopic bands of GM are slightly brighter than the normal cortex, perhaps due to a looser packing of neurons after the disruption of neuronal migration (LoTurco & Bai, 2006). The slightly higher signal intensity as compared to normal cortex shifts these areas of SBH into the range of the filter defined in step 3 of our method. As a consequence, they are highlighted in the junction image (cf. Fig. 2, rows 2 and 4). In case of very thin bands of heterotopic GM with a width of about two to three voxels (e.g., in patient 6), a partial volume effect could also contribute since a mixture of gray and white matter within one voxel would lead to higher net signal intensity. With both malformations, that is, FCD and SBH, being highlighted by the junction images, the differentiation is based on the location and appearance of the highlighted areas, that is, subcortical and bandlike structures in SBH in contrast to the gray–white matter junction in FCD.

In a population of about 500 patients with focal epilepsy systematically investigated at the Swiss Epilepsy Centre within 20 months, 5 patients showed signs of SBH in their MRI. Two additional patients were identified in two other epilepsy centers. The diagnosis of SBH has to rely on neuroradiological grounds only since for none of these patients a genetic or histological validation is currently available. However, this is not unusual since surgical resection of epileptogenic tissue in this commonly diffuse and bilateral syndrome is normally not recommended in view of

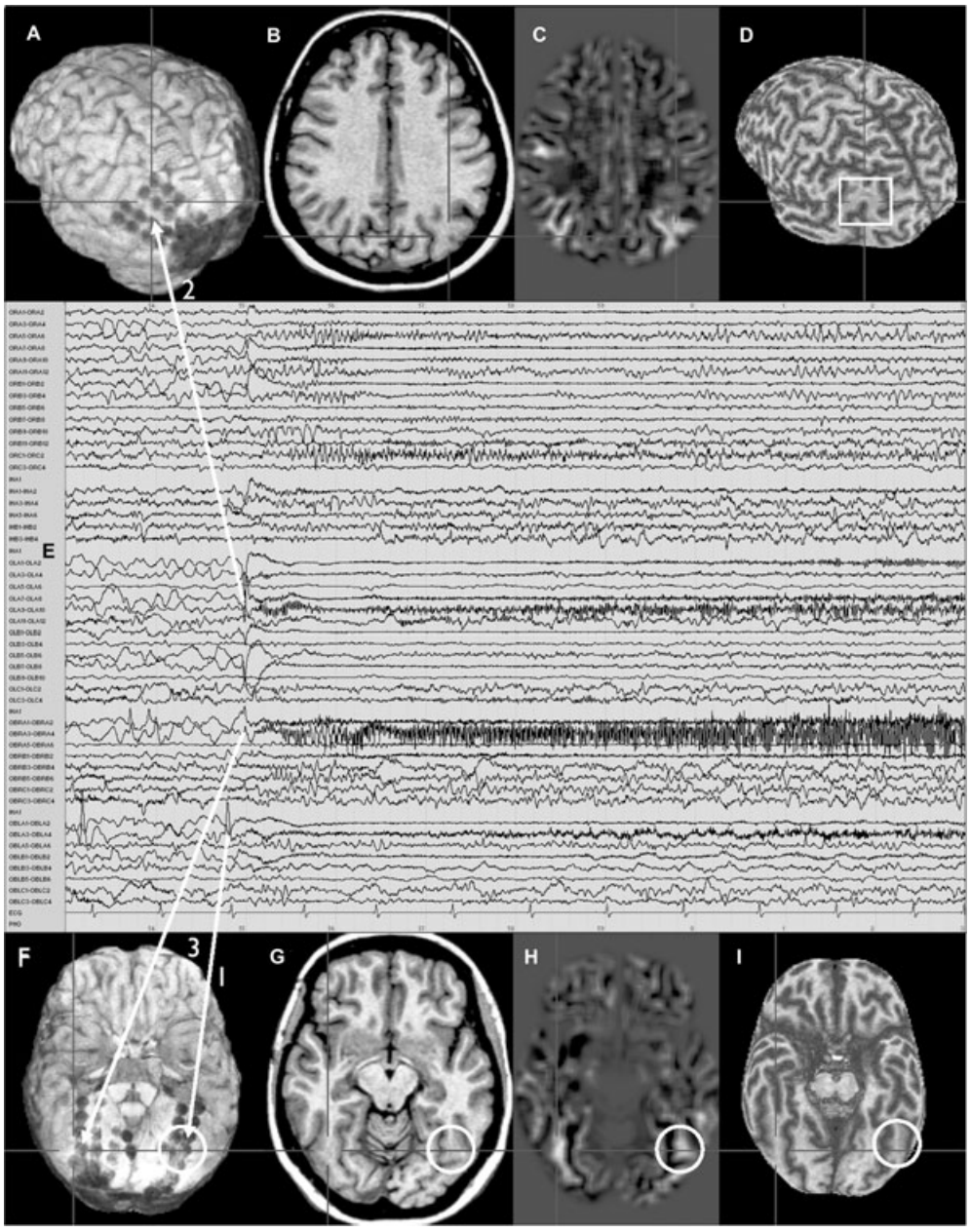

Figure 6.
Results of invasive EEG recordings in patient 7 showing the positions of implanted strip electrodes (**A** and **F**), corresponding planar T_1 images (**B** and **G**) and junction images (**C** and **H**), curvilinear reformatted images in about 10 mm depth from the cortical surface (**D** and **I**) together with the EEG curves (**E**). The crosshairs in subfigures **A–D** and **F–I**, respectively, are coupled and point to the same location. The seizure starts in the left basal temporooccipital region (white arrow No.1, white circles) before involving within the next 200 ms ipsilateral parieto-occipital areas (white arrow No. 2) and the contralateral basal temporooccipital region (white arrow No. 3). Both the seizure onset zone and the propagation areas match with those brain regions where the results of MRI postprocessing have indicated SBH. Please note in subfigure **D** that the curvilinear reformatted image also shows a bandlike structure (white square) circling around the sulcus directly below the electrode contact in subfigure A involved in the early seizure propagation (white arrow No. 2). The curvilinear reformatted image of subfigure **I** also indicate blurring of the gray–white matter junction in the same basal temporooccipital regions highlighted in the adjacent junction image (H).

poor postoperative outcome (Bernasconi et al., 2001b). On the other hand, genetic analysis is fruitless in many cases, probably because of miscellaneous underlying and partly still unknown mutations (D'Agostino et al., 2002). Nevertheless, the posterior predominance of SBH in our patients with partial double cortex syndrome is in line with the distribution of SBH observed in patients with missense mutations of the *LIS1* gene (Pilz et al., 1999; Kato & Dobyns, 2003; Leventer, 2005). Less severe forms of SBH may result from somatic mosaic mutations that have also been described for the *LIS1* gene (Sicca et al., 2003). The clinical spectrum of SBH ranging from clearcut cases to those that are hardly recognizable on conventional MR images may be explained by variable rates of mosaicism. It has to be noted that the initial ictal symptoms in the majority of our patients (i.e., hemianopsia, numbness of hand and arm, eye blinking, eye deviation, metamorphopsia, and visual illusions) can be attributed to posterior brain regions, which correlates very well with the distribution of SBH in these patients.

Retrospectively, some of the lesions detected by voxel-based MRI analysis appear to be quite obvious, even in the conventional T_1-weighted images (Fig. 3). It has to be taken into account, however, that these T_1 images of only 1-mm slice thickness have been especially selected to depict the malformations as clearly as possible and to illustrate their extent. In the other MR sequences, that is, T_2- or FLAIR-weighted images, these lesions were far less recognizable if at all. The T_1-weighted images, on the other hand, are derived from a volume data set consisting of 150–180 slices. A thorough inspection of this large search space in different angulations requires special attention, patience, and time. Frequently, the T_1-weighted sequences are acquired in the sagittal plane and only used as a basis for axial and coronar reconstructions with thicker slices of 3–5 mm, which impedes the detection of subtle lesions. Furthermore, there were additional obstacles prohibiting an initial discovery of the malformations. In patient 3, for example, the previous MRI investigations had been compromised by motion artifacts that to a lesser extent are also visible in the T_1 images in Fig. 3. The identification of SBH can also be difficult because of their symmetry (Barkovich et al., 1989). In patient 5, the broad and bilateral symmetrical band heterotopia in the posterior brain regions were confounded with unspecific signal alterations of WM. The small lines of WM dividing normal cortex and underlying heterotopic GM were not recognized at first sight. In these cases, MRI postprocessing guided the attention to those findings that became crucial for establishing the correct diagnosis. Apart from the heterotopia, which (retrospectively) may appear to be well recognizable in the T_1-weighted images, voxel-based MRI analysis also highlighted regions with only very thin and incontinuous SBH, which are still difficult to detect even when knowing the diagnosis (please cf. patient 4). This helps to assess the extent of these malformations and to verify their bilateral distribution, even in cases with regional predominance.

The diagnosis in patient 7 is controversial among the authors and other imaging experts who have studied the MRI. Some of them, mostly professional neuroradiologists, do not think that the findings in the conventional T_1-weighted images allow for the diagnosis of a double cortex syndrome. The abnormalities in the posterior brain regions could be, for example, unspecific WM alterations. However, there are arguments in favor of the SBH hypothesis. The abnormalities highlighted by voxel-based MRI analysis are in perfect agreement with the bilateral posterior seizure origin proven by noninvasive and invasive EEG findings as well as indicated by the ictal symptoms. Pure WM lesions, on the contrary, would not explain the seizures. In addition, in the enlarged high-resolution T_1 images (Fig. 5, row 5, white circles marked by arrows), these structures partly show imaging properties that are generally regarded as characteristic aspects of SBH (i.e., band-like structures lying parallel to the gray–white matter junction and divided from the cortical mantle by a thin layer of WM) (Barkovich et al., 1989). But these findings are very subtle, and the width of these structures only spans over one to three voxels, thus reaching the limits of spatial resolution of current MRI. It cannot be excluded that some other kind of cortical malformation (e.g., FCD) is present. In view of the bilateral distribution, however, FCD seems to be less probable than SBH. But even if it is not SBH, it has to be noted that the MRI postprocessing has been the only diagnostic method so far that has pointed to a possible underlying etiology in this patient.

The relatively high prevalence of SBH in the patients systematically investigated at the Swiss Epilepsy Centre and the fact that the diagnoses in three out of five patients in Zurich were only found after MRI postprocessing gives the impression that subtle forms of SBH perhaps are currently underrecognized by conventional MRI. The voxel-based MRI analysis presented here could aid in finding the underlying etiology in cases of previously cryptogenic epilepsy by enhancing image properties not readily accessible by visual analysis of conventional MRI. The history of patient 3 points to the necessity of optimal imaging at the earliest stages of presurgical evaluation. Detection of lesions precluding patients from epilepsy surgery can prevent them from the performance of potentially harmful diagnostic procedures (such as the Wada test or invasive EEG recordings). Even more relevant, optimal imaging can prevent the performance of surgeries without realistic chance for seizure freedom.

The idea of assisting lesion detection by image postprocessing strategies is increasingly recognized. A variety of MR postprocessing techniques has been proposed in the past years (Sisodiya et al., 1995; Woermann et al., 1999; Fischl & Dale, 2000; Bernasconi et al., 2001a; Antel et al.,

2002; Kassubek et al., 2002; Merschhemke et al., 2003; Wilke et al., 2003; Huppertz et al., 2005). The voxel-based technique presented here allows a comprehensive 3D analysis of volumetric MRI data, which may reveal abnormalities that are not visible when the data are viewed as two-dimensional images only and which is less prone to misinterpretation due to partial volume effects. In addition, an inherent comparison with a normal database is included to compensate for physiological variations of the gray–white matter transition in different brain regions. It has to be mentioned that our normal database comprised MRI data from five different MRI scanners with different field strength. This was only possible due to the "unified segmentation" algorithm introduced in SPM5 whereby image registration, tissue classification, and bias correction are integrated within the same model (Ashburner & Friston, 2005). A scanner-specific T_1-weighted template for normalization as used in SPM2 and SPM99 is no longer required; the algorithm is only based on templates for GM, WM, and CSF. For theoretical reasons, the unified segmentation is less dependent on scanner-specific templates, and recent empirical results already suggest that normalization results using the unified model are superior to standard nonlinear approaches used previously (Crinion et al., 2007). We have chosen to integrate data from different MR scanners in order to be able to analyze MRIs from different sources even if no comparative data from the same scanner are available. In our experience, the theoretical disadvantage of not using a scanner-specific normal database is outweighed by the fact that our combined database is larger (currently 150 MRI control data sets) and thus a better model for the variability in the normal population. However, this strategy is only used to highlight possible abnormal brain regions in single patients. We do not mean to imply that this is also correct for group comparisons with statistical testing of certain hypotheses.

The calculation of the new feature map (i.e., the junction image) is completely automated and observer independent. It is applicable to T_1-weighted images of both 1.5 and 3T MR scanners. The script employs standard procedures of SPM5 and additional simple computations done by the image calculation tool of SPM5. Except for the commercial MATLAB platform required for SPM, the method is thus based on freely available software. However, the key steps of this method (i.e., normalization, segmentation, filtering) could principally also be realized in other image-processing environments that are freeware such as, for example, the FMRIB Software Library (FSL; http://www.fmrib.ox.ac.uk/fsl) or the AFNI software (http://www.afni.nimh.nih.gov/afni), thus sparing the MATLAB licence.

In conclusion, the results of this study suggest that a considerable part of cases with SBH remains unrecognized by conventional MRI. The voxel-based MRI analysis presented here may help to identify subtle forms of SBH and to increase the sensitivity of MRI. Thereby, it appears to be a valuable additional diagnostic tool in the evaluation of patients with cryptogenic epilepsy.

Acknowledgments

We are grateful for the valuable comments of Prof. Dr. R. Guerrini (Pediatric Hospital A. Meyer-University of Florence, Italy) on the MR images of our patients. The development of the MRI postprocessing technique presented here was kindly supported by the Olga Mayenfisch-Stiftung, Zurich.

Conflict of interest: We confirm that we have read the Journal's position on issues involved in ethical publication and affirm that this report is consistent with those guidelines. We declare that there are no conflicts of interest.

References

Antel SB, Bernasconi A, Bernasconi N, Collins DL, Kearney RE, Shinghal R, Arnold DL. (2002) Computational models of MRI characteristics of focal cortical dysplasia improve lesion detection. *Neuroimage* 17:1755–1760.

Ashburner J, Friston KJ. (2005) Unified segmentation. *Neuroimage* 26:839–851.

Barkovich AJ, Jackson DE, Jr., Boyer RS. (1989) Band heterotopias: a newly recognized neuronal migration anomaly. *Radiology* 171:455–458.

Barkovich AJ, Kuzniecky RI. (2000) Gray matter heterotopia. *Neurology* 55:1603–1608.

Barkovich AJ, Kuzniecky RI, Jackson GD, Guerrini R, Dobyns WB. (2005) A developmental and genetic classification for malformations of cortical development. *Neurology* 65:1873–1887.

Bernasconi A, Antel SB, Collins DL, Bernasconi N, Olivier A, Dubeau F, Pike GB, Andermann F, Arnold DL. (2001a) Texture analysis and morphological processing of magnetic resonance imaging assist detection of focal cortical dysplasia in extra-temporal partial epilepsy. *Ann Neurol* 49:770–775.

Bernasconi A, Martinez V, Rosa-Neto P, D'Agostino D, Bernasconi N, Berkovic S, MacKay M, Harvey AS, Palmini A, da Costa JC, Pagliloli E, Kim HI, Connolly M, Olivier A, Dubeau F, Andermann E, Guerrini R, Whisler W, Toledo-Morrell L, Morrell F, Andermann F. (2001b) Surgical resection for intractable epilepsy in "double cortex" syndrome yields inadequate results. *Epilepsia* 42:1124–1129.

Crinion J, Ashburner J, Leff A, Brett M, Price C, Friston K. (2007) Spatial normalization of lesioned brains: performance evaluation and impact on fMRI analyses. *Neuroimage* 37:866–875.

D'Agostino MD, Bernasconi A, Das S, Bastos A, Valerio RM, Palmini A, Costa DC, Scheffer IE, Berkovic S, Guerrini R, Dravet C, Ono J, Gigli G, Federico A, Booth F, Bernardi B, Volpi L, Tassinari CA, Guggenheim MA, Ledbetter DH, Gleeson JG, Lopes-Cendes I, Vossler DG, Malaspina E, Franzoni E, Sartori RJ, Mitchell MH, Mercho S, Dubeau F, Andermann F, Dobyns WB, Andermann E. (2002) Subcortical band heterotopia (SBH) in males: clinical, imaging and genetic findings in comparison with females. *Brain* 125:2507–2522.

Fischl B, Dale AM. (2000) Measuring the thickness of the human cerebral cortex from magnetic resonance images. *Proc Natl Acad Sci USA* 97:11050–11055.

Huppertz HJ, Grimm C, Fauser S, Kassubek J, Mader I, Hochmuth A, Spreer J, Schulze-Bonhage A. (2005) Enhanced visualization of blurred gray-white matter junctions in focal cortical dysplasia by voxel-based 3D MRI analysis. *Epilepsy Res* 67:35–50.

Huppertz HJ, Kassubek J, Altenmueller DM, Breyer T, Fauser S. (2007) Automatic curvilinear reformatting of three-dimensional MRI data of the cerebral cortex. *Neuroimage* (in press). Epub ahead of print.

Kassubek J, Huppertz HJ, Spreer J, Schulze-Bonhage A. (2002) Detection and localization of focal cortical dysplasia by voxel-based 3-D MRI analysis. *Epilepsia* 43:596–602.

Kato M, Dobyns WB. (2003) Lissencephaly and the molecular basis of neuronal migration. *Hum Mol Genet* 1:R89–R96.

Kovalev D, Spreer J, Honegger J, Zentner J, Schulze-Bonhage A, Huppertz HJ. (2005) Rapid and fully automated visualization of subdural electrodes in the presurgical evaluation of epilepsy patients. *AJNR Am J Neuroradiol* 26:1078–1083.

Leventer RJ. (2005) Genotype-phenotype correlation in lissencephaly and subcortical band heterotopia: the key questions answered. *J Child Neurol* 20:307–312.

LoTurco JJ, Bai J. (2006) The multipolar stage and disruptions in neuronal migration. *Trends Neurosci* 29:407–413.

Merschhemke M, Mitchell TN, Free SL, Hammers A, Kinton L, Siddiqui A, Stevens J, Kendall B, Meencke HJ, Duncan JS. (2003) Quantitative MRI detects abnormalities in relatives of patients with epilepsy and malformations of cortical development. *Neuroimage* 18:642–649.

Palmini A, Andermann F, Aicardi J, Dulac O, Chaves F, Ponsot G, Pinard JM, Goutieres F, Livingston J, Tampieri D. (1991) Diffuse cortical dysplasia, or the 'double cortex' syndrome: the clinical and epileptic spectrum in 10 patients. *Neurology* 41:1656–1662.

Pilz DT, Kuc J, Matsumoto N, Bodurtha J, Bernadi B, Tassinari CA, Dobyns WB, Ledbetter DH. (1999) Subcortical band heterotopia in rare affected males can be caused by missense mutations in DCX (XLIS) or LIS1. *Hum Mol Genet* 8:1757–1760.

Rorden C, Brett M. (2000) Stereotaxic display of brain lesions. *Behav Neurol* 12:191–200.

Sicca F, Kelemen A, Genton P, Das S, Mei D, Moro F, Dobyns WB, Guerrini R. (2003) Mosaic mutations of the LIS1 gene cause subcortical band heterotopia. *Neurology* 61:1042–1046.

Sisodiya SM, Free SL, Fish DR, Shorvon SD. (1995) Increasing the yield from volumetric MRI in patients with epilepsy. *Magn Reson Imaging* 13:1147–1152.

Tzourio-Mazoyer N, Landeau B, Papathanassiou D, Crivello F, Etard O, Delcroix N, Mazoyer B, Joliot M. (2002) Automated anatomical labeling of activations in SPM using a macroscopic anatomical parcellation of the MNI MRI single-subject brain. *Neuroimage* 15:273–289.

Wilke M, Kassubek J, Ziyeh S, Schulze-Bonhage A, Huppertz HJ. (2003) Automated detection of gray matter malformations using optimized voxel-based morphometry: a systematic approach. *Neuroimage* 20:330–343.

Woermann FG, Free SL, Koepp MJ, Ashburner J, Duncan JS. (1999) Voxel-by-voxel comparison of automatically segmented cerebral gray matter–a rater-independent comparison of structural MRI in patients with epilepsy. *Neuroimage* 10:373–384.